Shear strain in carbon nanotubes under hydrostatic pressure

S. Reich, H. Jantoljak, and C. Thomsen

Institut für Festkörperphysik, Technische Universität Berlin, Hardenbergstrasse 36, D-10623 Berlin, Germany

We investigated the hydrostatic and shear strain components introduced in the graphite hexagons by applying hydrostatic pressure to single-walled carbon nanotubes. The vibrational modes are expected to show different pressure derivatives depending on the polarization of the eigenvector with respect to the nanotube axis, but independent of chirality. A comparison with tight-binding calculations allows us to estimate the Grüneisen parameter (1.24) and the shear phonon deformation potentials (0.41); they compare favorably with experimental results on nanotubes.

The study of vibrational modes under pressure has been of recent interest when studying the elastic properties of single and multiwalled carbon nanotubes and comparing them to theoretical predictions. It was found that the influence of bundleing on single-walled tubes is large[1–5] and that multiwalled tubes may be described within the same elasticity model as single-walled tubes.[6] Calculations of the elastic constants were provided by several groups[7–9] and appear to agree with experiment in the magnitude of the observed frequency shifts. However, since nanotubes are highly anisotropic, uniaxial structures, the strain resulting from hydrostatic pressure is, in general, different for the length and the circumference of the tube; the strain tensor has two independent components.[10] Consequently, under hydrostatic pressure one would expect different pressure slopes for modes vibrating parallel and perpendicular to the axis, which has not yet been reported.

Single-walled nanotubes are formed by rolling up a graphene sheet to a long, narrow cylinder. The vibrational and electric properties of the tubes are determined by their diameter and chirality, i.e., the angle Θ between the carbon bonds and the tube axis. There is an ongoing controversy about the distribution of chiralities in real nanotubes samples ranging from Θ being always within $\approx 10°$ around the armchair direction to a random distribution of chiralites.[11] Typically the vibrations of carbon nanotubes are investigated by Raman spectroscopy. Single-walled tubes show scattering by the radial breathing mode with a van der Waals contribution in the low-energy region (150–200 cm^{-1}) and by the high-energy modes (≈ 1600 cm^{-1}), where the carbon atoms move out of phase in the axial or circumferential direction. To a good approximation the frequencies of these high-energy vibrations can be related to those of graphite via zone folding, although the curvature of the graphene sheet introduces a softening of the modes.[9,12] For excitation between 1.7 and 2.2 eV, the modes of metallic nanotubes are resonantly enhanced, the resonances for semiconducting tubes are above and below that.[13,14] So far, only the pressure dependence of semiconducting single-walled nanotubes has been reported.[1,6,15] Surprisingly, all groups found the pressure derivatives of the different high-energy modes to be similar, i.e., the expected splitting appears to be absent.

In this paper we show that hydrostatic pressure applied to carbon nanotubes results in a nonhydrostatic deformation of the graphite hexagons. By making reference to the rolled up graphene sheet we obtain the Grüneisen parameter and the shear strain phonon deformation potentials with the help of recent tight-binding calculations. We compare our values with graphite and high-pressure experiments on nanotubes.

In a recent paper, Damnjanović *et al.*[16] derived the line groups, which, similar to space groups in three dimensions, describe the full symmetry of a one-dimensional system, and the corresponding point groups for carbon nanotubes. According to them, the point group for chiral nanotubes is D_q, and D_{qh} for the achiral zigzag and armchair tubes, q being the number of graphene cells in the elementary cell of the tube. The strain tensor in these point groups reduces to $\Gamma(\varepsilon) = 2A_{1(g)} \oplus E_{1(g)} \oplus E_{2(g)}$, the index g holding for the achiral tubes. Only the two fully symmetric strain components can be induced by hydrostatic pressure.[10] They describe a strain ε_{zz} along the axis and $\varepsilon_{\theta\theta}$ along the circumference. Although these components are fully symmetric in the point groups of the tubes, they are not for the underlying graphene hexagon. Consider unwrapping the tube to a long and narrow rectangle, the longer side being parallel to the tube axis z and the shorter one to the circumference of the tube θ. The strain in this graphene sheet due to $\varepsilon_{\theta\theta}$ and ε_{zz} now reads

$$\varepsilon = \begin{pmatrix} \varepsilon_{\theta\theta}\cos^2\Theta + \varepsilon_{zz}\sin^2\Theta & \frac{1}{2}\sin(2\Theta)(\varepsilon_{zz} - \varepsilon_{\theta\theta}) \\ \frac{1}{2}\sin(2\Theta)(\varepsilon_{zz} - \varepsilon_{\theta\theta}) & \varepsilon_{\theta\theta}\sin^2\Theta + \varepsilon_{zz}\cos^2\Theta \end{pmatrix};$$
(1)

where we transformed ε to the principal axes of graphene, Θ being the chiral angle. For clarity the out-of-plane component was omitted; it factorizes out in the sheet. Obviously, the deformation of the graphene elementary cell given in Eq. (1) is not hydrostatic for any chirality and will cause a splitting of the doubly degenerate E_{2g} graphene mode. For the nanotubes this yields different pressure derivatives for modes vibrating in axial and circumferential direction.

The dynamical equation for the phonon modes in the presence of strain is given by[17]

$$m\ddot{u}_i = -\left(m\omega_0^2 u_i + \sum_{klm} K_{ikml}^{(1)}\varepsilon_{lm}u_k \right);$$
(2)

where u is the displacement of the atoms, m is their mass, and ω_0 the strain-free frequency. The second summand describes the change in phonon frequency due to the strain. The symmetric tensor $K^{(1)}$ has only three nonzero components because of the hexagonal symmetry of the graphene sheet, namely,[10]

$$K_{1111}=K_{2222}=m\tilde{K}_{11}$$

$$K_{1122}=m\tilde{K}_{12}$$

$$K_{1212}=m\frac{1}{2}(\tilde{K}_{11}-\tilde{K}_{12}). \qquad (3)$$

From Eqs. (2) and (3) the secular equation can be constructed,[17,18] the solutions of which give the frequencies in the strained sheet. With the strain tensor given in Eq. (1) the relative shift in the phonon frequencies $\Delta\omega/\omega_0$ is

$$\frac{\Delta\omega}{\omega_0}=\frac{(\tilde{K}_{11}+\tilde{K}_{12})}{4\omega_0^2}(\varepsilon_{\theta\theta}+\varepsilon_{zz})\pm\frac{1}{2}\frac{(\tilde{K}_{11}-\tilde{K}_{12})}{2\omega_0^2}(\varepsilon_{\theta\theta}-\varepsilon_{zz}). \qquad (4)$$

The first phonon deformation potential $(\tilde{K}_{11}+\tilde{K}_{12})/4\omega_0^2=-\gamma$ is the Grüneisen parameter, which describes the frequency shift under hydrostatic strain. The splitting of the modes under the shear strain components comes from the second term. For the nanotube high-energy modes, γ is expected to be similar to the one in graphite, since the effect of curvature on frequencies is on the order of 10^{-2}.[12] Likewise, both phonon-deformation potentials have the same value for the three high-energy vibrations, because these modes differ only in the confinement wave vector along the circumference of the tube. The shift $\Delta\omega/\omega_0$ is independent of chirality; instead, it depends only on the polarization direction of a given phonon eigenvector.

The pressure dependence of the nanotube modes was calculated for armchair tubes and ropes of armchair tubes by Kahn and Lu[4] and by Venkateswaran et al.[1] Since the displacement of the high-energy modes in armchair tubes is either circumferential (A_{1g}, E_{2g}) or axial (E_{1g}) by symmetry, different slopes are expected when a shear strain is present in the graphite hexagon. In the tight-binding calculation of Ref. 4 a hydrostatic pressure was approximated by stressing an entire nanorope in the basal plane. The volume change of the relaxed structure was then related to the pressure by $\Delta V/V=\varepsilon_z+2\varepsilon_x=p/B_{\text{rope}}$. In Fig. 1 we show the calculated frequency shift of the three high-energy modes normalized to the strain-free frequency, which we obtained from Fig. 5 in the reference. The slopes of the two circumferential modes are slightly different (0.5 TPa^{-1}), while the axial E_{1g} mode is split off by 1.3 and 1.8 TPa^{-1} from the E_{2g} and A_{1g} modes, respectively. The mean hydrostatic shift (6.18 TPa^{-1}) is shown as a dashed line in the figure; the average shear-strain splitting is $\Delta\omega_{\text{sp}}/\omega_0=1.55$ TPa^{-1}. The bulk modulus of a nanorope has two contributions accounting for the van der Waals interaction between the tubes and the stiffness of a single tube. To a good approximation only the latter has to be considered for the high-energy modes, yielding $\Delta\omega_{\text{h}}/\omega_0=6.18$ $\text{TPa}^{-1}=\gamma p/B_{\text{tube}}$ ($B_{\text{tube}}=0.2$ TPa) (Ref. 7) and the Grüneisen parameter $\gamma=1.24$
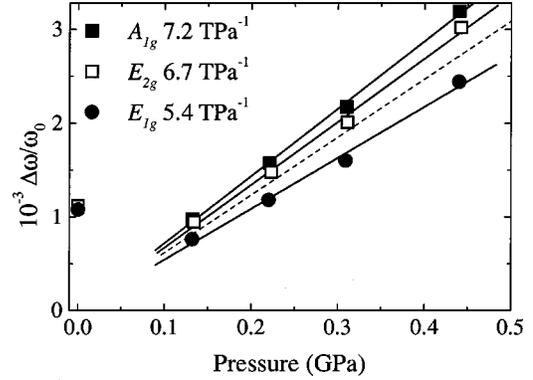
FIG. 1. Calculated shift of the high-energy modes of armchair nanotubes versus applied pressure. The data were taken from Ref. 4 and normalized to the frequency at ambient pressure. The calculated point at 0 GPa was omitted from the linear regressions.

(see Table I). This is in good agreement with the values measured in graphite under hydrostatic pressure[19] normalized to a two-dimensional sheet $\gamma=-d\ln\omega/2d\ln a$, a being the in-plane lattice constant of graphite.

To derive the shear strain phonon deformation potential a closer look at the strain introduced in a single nanotube by a basal stress is necessary. A stress in the (x,y) plane results in a decrease in diameter but in an increase in length given by $\varepsilon_z=-(2C_{13}/C_{33})\varepsilon_x=-0.29\varepsilon_x$.[10,7] With the volume change given above and Eq. (4), the full splitting of the slopes $\Delta\omega_{\text{sp}}/\omega_0$ is

$$\frac{\Delta\omega_{\text{sp}}}{\omega_0}=\frac{(\tilde{K}_{11}-\tilde{K}_{12})}{2\omega_0^2}\frac{(1+2C_{13}/C_{33})}{(2-2C_{13}/C_{33})}p/B_{\text{tube}}, \qquad (5)$$

and $(\tilde{K}_{11}-\tilde{K}_{12})/2\omega_0^2=0.41$. In Table I we listed for comparison the values of the shear deformation potential measured in a graphitic fiber under uniaxial stress along the fiber axis, which is about 3 times higher.[20] There is, however, a similar factor between the Grüneisen parameter obtained in these measurements and the more precise value measured later under hydrostatic pressure.[19] If we scale the shear deformation potential by the ratio of the two γ we find $(\tilde{K}_{11}-\tilde{K}_{12})/2\omega_0^2=0.64$, close to the value calculated for armchair nanotubes.[21]

In contrast to the basal stress assumed by Kahn and Lu, the molecular dynamics simulations by Venkateswaran et

TABLE I. The phonon deformation potentials of nanotubes, graphite, and a graphitic fiber, all normalized to a two-dimensional plane.

	γ	$\dfrac{(\tilde{K}_{11}-\tilde{K}_{12})}{2\omega_0^2}$
nanotubes	1.24	0.41
graphite [a]	1.59	
graphitic fiber [b]	2.87	1.13

[a]Reference 19.
[b]Reference 20.

TABLE II. Strain induced by hydrostatic pressure in the circumferential ($\varepsilon_{\theta\theta}$) and axial ($\varepsilon_{zz}$) direction in single-walled nanotubes according to the three models described in the text. The expected hydrostatic frequency shift and the full shear strain splitting were calculated with Eq. (4) and the phonon deformation potentials of nanotubes given in Table I.

	$\varepsilon_{\theta\theta}/p$ (TPa^{-1})	ε_{zz}/p (TPa^{-1})	$\varepsilon_{\theta\theta}/\varepsilon_{zz}$	$\Delta\omega_{\mathrm{h}}/\omega_0$	$\Delta\omega_{\mathrm{sp}}/\omega_0$
Elastic constants [a]	-1.74	-0.49	3.5	2.8	0.3
Elasticity model [b]	-2.04	-1.07	1.9	3.9	0.4
Molecular dynamics [c]	-3.41	-0.91	3.7	5.4	1.0
graphite [d]	-0.8	-0.8			

[a]Reference 7.
[b]Reference 6.
[c]Reference 1.
[d]Reference 19.

al.[1] were performed for applied hydrostatic pressure. Unfortunately, only the pressure derivative of the E_{2g} armchair mode is given in the reference, but, as the authors state, they found a small difference in slopes as well. Another interesting piece of information can be determined by the data presented, namely, the strain in circumferential and axial direction in a nanotube under pressure. We extracted the values from Fig. 4 in Ref. 1, where the axial lattice constant and the radius as a function of pressure are presented; the values are given in Table II together with the results of two other approaches we chose. For the second approach we used the elastic continuum model worked out by us previously.[6] The parameters necessary within this model are the diameter of a tube $d=1.4$ nm, Poisson's ratio $\nu=0.16$, and Young's modulus $E=1$ TPa, the latter two we took from *ab initio* calculations.[9] Finally, we determined the two independent strain components with the elastic constants found by Lu.[7] The values for the C_{ij} given in Table 4 of Ref. 7 were calculated for multilayered nanotubes, but, as Lu states, the change compared to single-walled tubes is small for the first few layers. We chose the two-layer (10,10) tube, since its radius is typical for nanotube samples. All three models agree in that both length and radius are reduced under pressure, the axial strain being smaller than the radial or circumferential one. When comparing the volume change of nanotubes $\varepsilon_{\theta\theta}+\varepsilon_{zz}$ under pressure, i.e., neglecting shear strain, to the one of graphite within the layer planes (see Table II), it is apparent that the higher pressure derivatives found in nanotubes are mostly due to the 2–3 times higher linear compressibility in the radial tube direction, resulting in a larger volume change for the same pressure.

With the help of the phonon deformation potentials, the hydrostatic shift $\Delta\omega_{\mathrm{h}}/\omega_0$ and the full shear strain splitting $\Delta\omega_{\mathrm{sp}}/\omega_0$ predicted by the three models are now readily obtained with Eq. (4). The published pressure derivatives of semiconducting tubes vary between 3.3–3.8 TPa^{-1}, but where more than one slope was reported[1,6] they agree to within 0.1 TPa^{-1}.[22] We performed Raman scattering on metallic tubes under pressure, i.e., using an excitation energy of 1.91 eV in the region of the metallic resonance. The frequencies are presented in Fig. 2 as a function of pressure; details of the experimental setup are given in Ref. 6. The analysis of the data is difficult due to the close proximity of the modes. Additionally, under pressure, the broadening of the peaks leads to a merging of the lines (see insets in Fig. 2). Never-

theless, when fitting the high-energy peak with three similarly sized Lorentzians or with a focus on the low and high-energy flanks for pressures up to 10 GPa, we find a splitting of 0.56 TPa^{-1} between the peaks at 1544 and 1565 cm^{-1} and a hydrostatic shift of 3.8 TPa^{-1}. The third peak, at 1592 cm^{-1}, which has been assigned to semiconducting tubes (see Ref. 4 of Ref. 13 and Ref. 14), again has a pressure derivative of 3.8 TPa^{-1}.

It thus seems that only the hydrostatic part of the frequency shift is observed in semiconducting carbon nanotubes. In contrast to the higher symmetry achiral armchair or zigzag tubes, the phonon displacement in chiral tubes can have arbitrary directions with respect to the tube axis, because mirror planes are absent in their point groups. A distribution of phonon polarization directions averages out the splitting of the slopes introduced by a shear strain and results in an average mode shift.[23] Most likely, this is the reason why only the hydrostatic shift is observed, since chiral tubes are always present in real samples. Armchair tubes can only contribute to the metallic Raman spectra, thus the peaks at
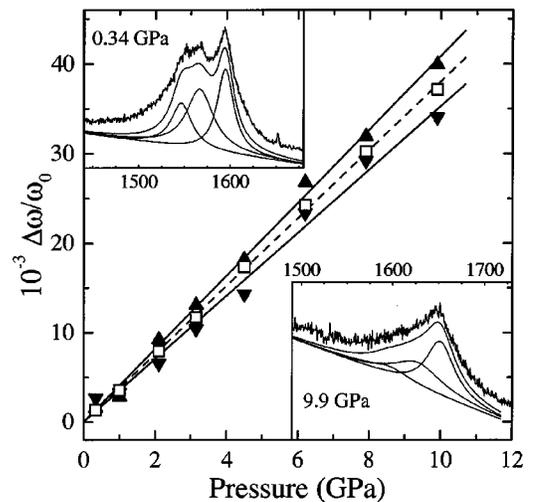
FIG. 2. Shift of the Raman active modes of metallic single-walled nanotubes versus applied pressure normalized to the frequency at zero pressure. The up triangles refer to the mode at 1565 cm^{-1} at ambient pressure, the down triangles to the one at 1544 cm^{-1}, and the open squares to the 1592 cm^{-1} mode. The insets show Raman spectra (Raman shift in cm^{-1}) at $p=0.34$ and 9.9 GPa and the fit to the data.

1544 and 1565 cm^{-1} are probably dominated by the higher symmetry armchair tubes, making the shear strain splitting observable in pressure experiments. The magnitudes of the measured frequency shifts compare well with the predicted slopes given in Table II, showing that the axial linear compressibility of carbon nanotubes is on the order of graphite, but higher in the radial direction. Since the elasticity model, where curvature effects are neglected, gives similar results as the two other approaches, the different compressibilities reflect the cylindrical geometry of carbon nanotubes.

We studied theoretically and experimentally the strain introduced in single-walled nanotubes by hydrostatic pressure. The two independent strain components in circumferential and axial direction were found to be different, their ratio lying between ≈ 2 and 3.5. Because of the splitting of the graphite E_{2g} mode under shear strain, different pressure derivatives are expected for axial and circumferential vibrations in carbon nanotubes. From a recent tight-binding calculation we derived the Grüneisen parameter and the shear strain phonon deformation potential and found good agreement with the values of graphite. Semiconducting tubes have pressure derivatives given by the hydrostatic strain components. We showed Raman results obtained on metallic tubes, which confirm the predicted shear strain splitting.

[1] U. D. Venkateswaran, A. M. Rao, E. Richter, M. Menon, A. Rinzler, R. E. Smalley, and P. C. Eklund, Phys. Rev. B **59**, 10 928 (1999).

[2] C. Thomsen, S. Reich, A. R. Goñi, H. Jantoljak, P. Rafailov, I. Loa, K. Syassen, C. Journet, and P. Bernier, Phys. Status Solidi B **215**, 435 (1999).

[3] J. R. Wood, M. D. Frogley, E. R. Meurs, A. D. Prins, T. Pejis, D. J. Dunstant, and H. D. Wagner, J. Phys. Chem. **103**, 10 388 (1999).

[4] D. Kahn and J. P. Lu, Phys. Rev. B **60**, 6535 (1999).

[5] M. J. Peters, L. E. McNeil, J. P. Lu, and D. Kahn, Phys. Rev. B **61**, 5939 (2000).

[6] C. Thomsen, S. Reich, H. Jantoljak, I. Loa, K. Syassen, M. Burghard, G. S. Duesberg, and S. Roth, Appl. Phys. A: Mater. Sci. Process. **69A**, 309 (1999).

[7] J. P. Lu, J. Phys. Chem. Solids **58**, 1649 (1997); Phys. Rev. Lett. **79**, 1297 (1997).

[8] E. Hernández, C. Goze, and A. Rubio, Appl. Phys. A: Mater. Sci. Process. **68A**, 287 (1999); V. N. Popov, V. E. Van Doren, and M. Balkanski, Solid State Commun. **114**, 395 (2000).

[9] D. Sánchez-Portal, E. Artacho, J. M. Soler, A. Rubio, and P. Ordejón, Phys. Rev. B **59**, 12 678 (1999).

[10] J. F. Nye, *Physical Properties of Crystals* (Oxford University Press, Oxford, England, 1979).

[11] A. Thess *et al.*, Science **273**, 483 (1996); L. Henrard, A. Loiseau, C. Journet, and P. Bernier, Eur. Phys. J. B **13**, 661 (2000).

[12] C. Thomsen, Phys. Rev. B **61**, 4542 (2000).

[13] M. A. Pimenta, A. Marucci, S. A. Empedocles, M. G. Bawendi, E. B. Hanlon, A. M. Rao, P. C. Eklund, R. E. Smalley, G. Dresselhaus, and M. S. Dresselhaus, Phys. Rev. B **58**, R16 016 (1998).

[14] C. Thomsen, P. M. Rafailov, H. Jantoljak, and S. Reich, Phys. Status Solidi B (to be published).

[15] A. K. Sood, P. V. Teresdesai, D. V. S. Muthu, R. Sen, A. Govindaraj, and C. N. R. Rao, Phys. Status Solidi B **215**, 393 (1999).

[16] M. Damnjanović, I. Milošević, T. Vuković, and R. Sredanović, Phys. Rev. B **60**, 2728 (1999).

[17] F. Cerdeira, C. J. Buchenauer, F. H. Pollack, and M. Cardona, Phys. Rev. B **5**, 580 (1972).

[18] E. Anastassakis, in *Dynamical Properties of Solids*, edited by G. Horton and A. Maradudin (North-Holland, Amsterdam, 1980), Vol. 4, p. 157.

[19] M. Hanfland, H. Beister, and K. Syassen, Phys. Rev. B **39**, 12 598 (1989).

[20] H. Sakata, G. Dresselhaus, M. S. Dresselhaus, and M. Endo, J. Appl. Phys. **63**, 2769 (1988).

[21] The difference can be due to the stress determination in the fiber measurements. The constant factor between the assumed stress and the one actually present is then found in both phonon deformation potentials as can be seen from Eq. (4).

[22] The values are 3.4 and 3.5 TPa^{-1} (Ref. 1), 3.3 TPa^{-1} (Ref. 15), and 3.7, 3.7, and 3.8 TPa^{-1} (Ref. 6). To compare the different experiments we performed a linear regression on the data in contrast to the quadratic fit performed by Venkateswaran *et al.* Only the two modes which were observed up to 5 GPa were considered in Ref. 1.

[23] E. Anastassakis, J. Appl. Phys. **81**, 3046 (1997).